OXFORD

Cerebral Cortex, 2015, 1–9

doi: 10.1093/cercor/bhv065
Original Article

ORIGINAL ARTICLE

Intracortical Posterior Cingulate Myelin Content Relates to Error Processing: Results from T_1- and T_2-Weighted MRI Myelin Mapping and Electrophysiology in Healthy Adults

Håkon Grydeland, Lars T. Westlye, Kristine B. Walhovd, and Anders M. Fjell

Research Group for Lifespan Changes in Brain and Cognition, Department of Psychology, University of Oslo, Oslo, Norway

Address correspondence to Håkon Grydeland, Department of Psychology, University of Oslo, PO Box 1094 Blindern, 0317 Oslo, Norway. Email: hakon.grydeland@psykologi.uio.no

Abstract

Myelin content of the cerebral cortex likely impacts cognitive functioning, but this notion has scarcely been investigated in vivo in humans. Here we tested for a relationship between intracortical myelin and a direct measure of neural activity in the form of the electrophysiological response error-related negativity (ERN). Using magnetic resonance imaging, myelin mapping was performed in 81 healthy adults aged 40–60 years by means of a T_1- and T_2-weighted (T_1w/T_2w) signal intensity ratio approach. Error trials on a version of the Eriksen flanker task triggered the ERN, a negative deflection of the event-related potential reflecting performance monitoring. Compelling evidence from neuroimaging, lesion, and source localization studies indicates that the ERN stems from the cingulate cortex. Vertex-wise analyses across the cingulate demonstrated that increased amplitude of the ERN was related to higher levels of intracortical myelin in the left posterior cingulate cortex. The association was independent of general ability level and subjacent white matter myelin. The results fit the notion that degree of myelin within the posterior cingulate cortex as measured by T_1w/T_2w signal intensity plays a role in error processing and cognitive control through the relationship with neural activity as measured by ERN amplitude, potentially by facilitating local neural synchronization.

Key words: cingulate cortex, error-related negativity, event-related potentials, myelination, signal intensity

Introduction

Cerebral myelin, due to its impact on the speed and fidelity of nerve conduction (Hildebrand et al. 1993), likely constitutes a prime structural premise for optimal cognitive functioning. Still, in vivo mapping of cerebral myelin content to neural activity in humans remains sparse. Recorded at the scalp, the electroencephalography (EEG) has been taken to reflect transient neural synchrony within local brain patches, as well as across nonneighboring patches of such local synchrony (Girard et al. 2001; Varela et al. 2001; Voges et al. 2010; Palm et al. 2014). The amount of axon myelin may contribute importantly to this neural synchronization, which requires high levels of temporal precision (Nave 2010). Indeed, at the larger scale level, degree of white matter (WM) myelination has frequently been hypothesized as the premier neurobiological mechanism underlying individual differences in event-related potential (ERP) component amplitude and latency (Poulsen et al. 2007; Brydges et al. 2013). In Westlye et al. (2009), we demonstrated a relationship between the amplitude of the error-related negativity (ERN) (Falkenstein et al. 1991; Gehring et al. 1993) and fractional anisotropy (FA) derived from diffusion tensor imaging (DTI) in posterior parts of the cingulate

WM pathway. Thus, properties of WM related to myelin might play a role in the large-scale integration between distant brain sites of local synchronous activity, including the principal ERP generator. However, myelin also coats pyramidal axons in cortical circuits not going via deeper WM (Thomson and Bannister 2003; Tomassy et al. 2014). Interestingly, scalp-recorded EEG likely reflects summated field potentials caused by postsynaptic potentials of cortical pyramidal neurons (Luck 2005). Compared with the more large-scale integration effects of WM myelin, intracortical myelin might influence synchronization occurring within, or situated closer to, more localized networks of active generators, in turn influencing ERP amplitude (Thatcher et al. 1998; Elvsashagen et al. 2014). Moreover, the degree of intracortical myelin in a particular brain area appears to differ across individuals (Grydeland et al. 2013). Here, we ask how the variation in intracortical myelin mapped in vivo relates to variation in neural activity in humans.

To test the importance of interindividual differences in intracortical myelin for neural activity and cognitive processing, we use the ERN as the ERP component of interest. As studied here, the ERN denotes a negative deflection of the ERP peaking at fronto-central electrodes around 50–100 ms after self-generated, overt incorrect responses in a choice reaction time (RT) task, without external feedback indicating the presence of an error (Yeung et al. 2004; Hauser et al. 2014). This negativity putatively indexes activity in a cognitive control system monitoring performance (Taylor et al. 2007). Importantly, a host of studies indicate that ERN originates from the cingulate cortex (Dehaene et al. 1994; Debener et al. 2005; Agam et al. 2011). This feature enables strong a priori hypotheses concerning the location of effects. We performed intracortical myelin mapping using a ratio of T_1- and T_2-weighted (T_1w/T_2w) magnetic resonance imaging (MRI) signal intensity (Glasser and Van Essen 2011). This approach has been shown to map well with histological characterizations of myelin distribution (Glasser and Van Essen 2011) and to be sensitive to age-related differences across the lifespan as well as to RT variability (Grydeland et al. 2013). In accordance with source localization studies placing the neural generator of the ERN in the posterior cingulate (Agam et al. 2011), as well as our previous study showing a correlation between ERN amplitude and WM microstructural properties in the posterior part of the underlying cingulum tract (Westlye et al. 2009), we predicted stronger error signal (more negative ERN amplitude) with increased levels of intracortical myelin (larger T_1w/T_2w ratio value) in the posterior cingulate cortex.

To summarize, degree of myelin may be important for the transient local and global neural synchrony underlying the EEG signal recorded at the scalp. Results have indicated a relationship between integrity of the posterior cingulum WM bundle and ERN (Westlye et al. 2009), potentially reflecting myelin involvement important for the synchronization of activity between involved brain areas. The current study tests for additional effects of myelin in the overlying cingulate cortex, potentially important for synchronization of activity at, or closer to, the principal neuronal ERN generator.

Materials and Methods

A Regional Committee for Medical and Health Research Ethics approved the study. Details regarding recruitment and enrolment, experimental task, EEG recordings and processing, and ERN quantification have been reported in Westlye et al. (2009); MRI acquisition and T_1w/T_2w ratio maps generation have been described in Grydeland et al. (2013). The procedures were identical if not otherwise stated.

Briefly, written informed consent was obtained from all participants. We required participants to be right-handed, fluent Norwegian speakers, and have normal or corrected to normal vision and hearing. Exclusion criteria were self-reported neurological or psychiatric conditions known to affect normal cerebral functioning, including clinically significant stroke, traumatic brain injury, untreated hypertension, diabetes, use of psychoactive drugs within 2 years of the study, or worries concerning own cognitive status including memory function. All participants scored above 16 on Beck Depression Inventory (Beck and Steer 1987) and 26 or above on Mini Mental State Examination (Folstein et al. 1975).

Of the 87 participants included in Westlye et al. (2009), 6 participants were excluded here due to (number of participants in parentheses) corrupted (3) or nonidentical T_2w matrix (1), overfolding artifact (1), or incomplete T_2w data (1). Totally, we included 81 participants (48 females, 59.3%), mean age = 52.6 years, standard deviation (SD) = 5.1, min–max = 40.7–60.6).

General cognitive abilities were assessed by Wechsler Abbreviated Scale of Intelligence (Wechsler 1999). Estimated mean full-scale intelligence quotient (FIQ) was 113.7 (SD = 7.2, min–max = 95.5–128.1).

MRI was performed using a 12-channel head coil on a 1.5-T Siemens Avanto scanner (Siemens Medical Solutions, Erlangen, Germany). The T_1w volumes were acquired using a 3D T_1w MPRAGE: TR = 2400 ms, TE = 3.61 ms, TI = 1000 ms, 8° flip angle, FOV = 240 mm, matrix = 192 × 192 × 160, 1.25 × 1.25 × 1.2 mm voxels. For the T_2w volumes, we used a 3D T_2w sampling perfection with application-optimized contrasts using different flip angle evolutions (SPACE): TR = 3390 ms, TE = 388 ms, variable flip angle angle, FOV = 256 mm, 204 × 256 × 176 matrix, 1 mm isotropic voxels. Scans were acquired sagittally.

The T_1w volumes were processed using the Freesurfer 5.1 suite (http://surfer.nmr.mgh.harvard.edu), including brain extraction, intensity normalization, automated tissue segmentation, generation of white and pial surfaces, surface topology correction, and surface-based cortical thickness and mean curvature maps (Dale et al. 1999; Fischl and Dale 2000).

The T_2w image was registered to the T_1w image by using Freesurfer's *bbregister* (Greve and Fischl 2009), and FSL's *applywarp* tool using spline interpolation to minimize the WM and CSF contamination of GM voxels (Glasser and Van Essen 2011). The T_1w volume was divided on the aligned T_2w volume, creating a T_1w/T_2w ratio volume. We sampled T_1w/T_2w values vertex wise at a distance of 0.2 mm into the GM from the WM/GM boundary, yielding GM T_1w/T_2w surfaces. As we previously have found effects of WM microstructure quantified by DTI on ERN, we included measurements of WM T_1w/T_2w to be used as a per-vertex regressor in a follow-up model to assess for cortical-specific effects. To this end, similar to our previous studies (Westlye et al. 2010; Grydeland et al. 2013), we sampled T_1w/T_2w values at a 1.0 mm distance into the WM from the WM/GM boundary, yielding WM T_1w/T_2w surfaces. Further, the current imaging resolution does not allow for specific inferences at the level of cortical layers, which requires superior resolution and specific modeling (Waehnert et al. 2014). Still, in an effort to potentially allow more specific information regarding intraregional effects, we created 3 additional surfaces for each subject. Using a sliding window approach, the surfaces represented the average T_1w/T_2w values across 1) the first inner half of the cortex (from the WM/GM boundary and halfway into the cortex, or, in other terms, from 0 to 50% of the cortical thickness into the GM, sampled at 5% intervals), 2) the middle part of the cortex (from 25% to 75%

of the cortical thickness), and 3) the outermost half of the cortex (from 50% to 100% of the thickness). This attempt does still not allow us to infer about cortical layers, but might inform us in a relatively broad manner as to in what part of the GM the effects manifest. Thus, in total, we obtained 5 different T_1w/T_2w surfaces, 4 from the GM and 1 from WM, per hemisphere. Extreme T_1w/T_2w values [defined as values exceeding the following formula: first/third quartile −/+ (interquartile range * 5)] were set to the median value of the remaining vertices in each hemisphere.

The individual thickness, mean curvature, and T_1w/T_2w ratio surfaces were mapped to a common surface using a spherical averaging method to align cortical folding patterns (Fischl et al. 1999) and smoothed with a circularly symmetric Gaussian kernel (full width at half maximum = 12 mm). We divided the surface into 33 gyral-based areas in each hemisphere (Desikan et al. 2006) and merged the cingulate regions (caudal anterior, isthmus, posterior, and rostral anterior) into one 8586 and one 8041 vertices cingulate mask for the left and right hemisphere, respectively.

We administered a modified version of the Eriksen flanker task, similar to Debener et al. (2005) (Fig. 1A). Each trial consisted of a central fixation cross presented for a random interval ranging between 1200 and 1800 ms, followed by the presentation of 4 horizontal flanker arrows (length 1 cm or ~1°) in a vertical stack (2.5° high), pointing either to the left or the right, displayed centrally on a computer screen for 80 ms before a target arrow of the same size appeared in the middle of the stack for 30 ms. The flanker arrows were presented before the target to increase prepotent responding and to make the task more difficult. The participants were instructed to respond as accurately and quickly as possible by hand pressing a left button if the target middle arrow was pointing to the left and a right button if the target was pointing to the right. To increase the participants' motivation for rapid responses and to enhance their attentional investments in the task, a prompt instructing the participant to respond faster was displayed after every subsequent third trial including response omission, or after trials with RT exceeding 10% of the mean RT for the first 20 trials. The experiment consisted of 416 trials, with a short break half way, divided into "congruent" trials, where all arrows pointed in the same direction, and "incongruent" trials, where the middle arrow pointed in the opposite direction of the flanker arrows. The probability of an incongruent trial was 50% in a randomized fashion, with no more than 3 consecutive incongruent trials.

The electrophysiological recordings were carried out using the 128 channels EasyCap Montage No. 15 (http://www.easycap.de/easycap/), and a sampling rate of 1000 Hz, in a shielded Faraday chamber. The signals were amplified with Neuroscan SynAmps2 and filtered online with a 30-Hz low-pass and 0.15-Hz high-pass analog filter prior to digitalizing. All electrodes were referenced to a common electrode placed on the left mastoid. Vertical eye blinks were recorded with bipolar electrodes above and below the left canthi. Impedances were kept below 10 kΩ.

The continuous dataset was segmented into 1000 ms epochs from 600 ms prior to response. The entire epochs were linearly detrended and baseline corrected relative to activity from −600 to −500 ms prior to response. All trials with RT >600 ms were excluded, as were epochs containing signals ±100 μV. The epochs were corrected for eye blinks (Semlitsch et al. 1986) and digitally filtered with a 30-Hz, low-pass filter. Remaining epochs containing response-locked correct and erroneous responses from incongruent trials were extracted for further analysis. Mean number of accepted error trials was 44.7 (SD = 26.2, min–max = 10–135).

Based on mean grand average curves and topographical voltage plots for error trials for all participants, which revealed a maximum peak at channel FCz, we defined the peak amplitude of the ERN as the most negative point between 0 and 130 ms post-response at this channel (mean latency = 63.69 ms, SD = 22.32). Mean values from FCz, Fz, and Cz were used to represent the ERN to minimize single electrode noise and possible signal distortions. Individually adjusted average amplitude signal intensity was estimated by averaging the measured potential in the 20 ms preceding and 20 ms after peak amplitude at FCz for each

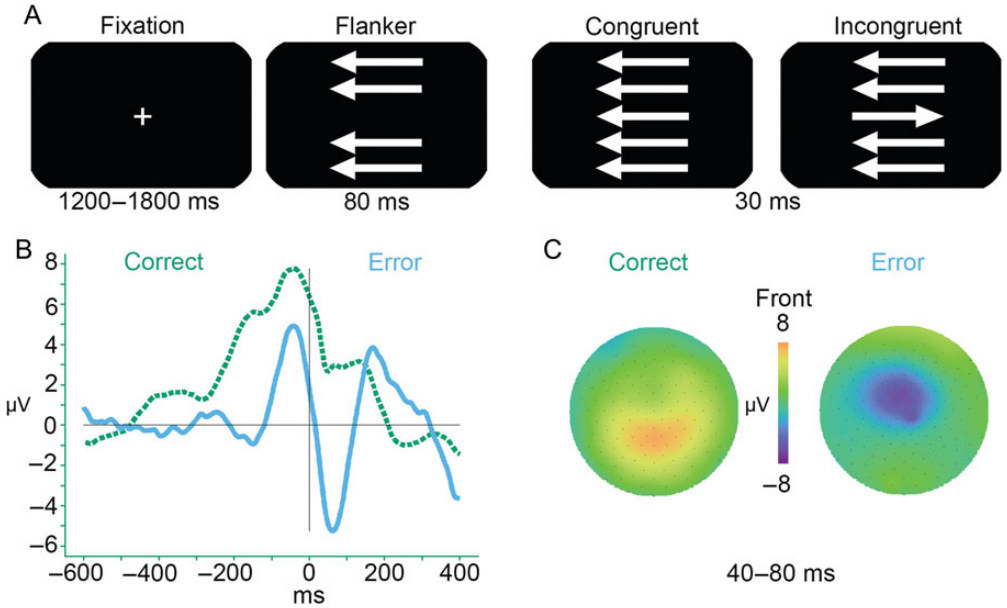

Figure 1. (A) Each trial consisted of a fixation cross followed by the presentation of 4 flanker arrows pointing to either the left or right side for 110 ms; during last 30 ms, the middle target arrow appeared together with the flanker arrows pointing either in the same (congruent condition) or the opposite (incongruent condition) directions with respect to the flanker arrows. (B) Grand average curves for mean Fz, FCz, and Cz activity demonstrating the ERN, the negative deflection peaking approximately 60 ms after error commission; response at time 0 ms. (C) Topographic distributions of the electrophysiological potentials after correct and erroneous responses.

participant. Mean amplitude for Fz, FCz, and Cz was –5.81 μV (SD = 5.50).

We applied a general linear model (GLM) in a vertex-wise manner to test for linear effects of ERN amplitude on the intracortical T_1w/T_2w ratio maps sampled at 0.2 mm into the GM. In addition to this main analysis, we performed additional surface-based GLMs to assess the specificity of the main result. In all GLMs, age and sex were used as global regressors, and cortical thickness as a per-vertex regressor, to control for possible confounding effects. The cortical thickness covariate was included to safeguard that the variation in T_1w/T_2w was not influenced by simultaneous variation in thickness. The data were tested against an empirical null distribution of maximum cluster size across 5000 iterations using Z Monte Carlo simulations as implemented in FreeSurfer (Hagler et al. 2006) synthesized with a cluster-forming threshold of $P < 0.01$ (2-sided), yielding clusters corrected for multiple comparisons. Following the existing literature clearly indicating a cingulate cortex generator of the ERN (Dehaene et al. 1994; Debener et al. 2005; Agam et al. 2011), we first performed the main analysis and correction within the entire cingulate cortex, as in Westlye et al. (2009). In an exploratory secondary approach, we repeated the main analysis across the entire cortex. The additional analyses across the cingulate cortex were as follows: First, to assess the potential effect of general ability level, we repeated the main analysis including FIQ as a regressor (and included FIQ in the remaining analyses). Second, in an attempt to control for potential biases associated with cortical folds, we also performed a GLM including a measure of the WM/GM boundary mean curvature as a per-vertex regressor. The third follow-up GLM was performed to test for the specificity of the intracortical effects compared with WM: We re-ran the main analysis adding WM T_1w/T_2w ratio as a per-vertex regressor. Finally, we ran a GLM for each of the 3 T_1w/T_2w surfaces sampled as an average of the inner half, middle half, and outer half of the GM from the WM/GM boundary to assess potential regional GM effects. In a final test of the specificity of the result from our main analysis, we compared the current T_1w/T_2w-ERN effect with WM-ERN effect obtained using DTI in Westlye et al. (2009) (see Westlye et al. for more details regarding DTI acquisition and analysis). To this end, we obtained the mean FA values from the significant cluster in Westlye et al. for the 81 subjects included here. These values were fed to a stepwise regression together with T_1w/T_2w values from the current main significant cluster corrected for thickness (residuals following linear regression of T_1w/T_2w values on thickness). To test for potential hemispheric differences in T_1w/T_2w and ERN amplitude correlations across the cingulate cortex, the *paired.r* function, part of the R (www.r-project.org/) package psych, was used.

To illustrate the individual data points and to provide a general measure of effect size, we extracted mean T_1w/T_2w values from significant cluster vertices in our main analysis, removed the effects of the nuisance regressors including FIQ, and plotted the residuals against ERN amplitude. To assess relationship with behavior, we also correlated these T_1w/T_2w values with number of correct responses and RT from the congruent and incongruent trials.

Results

Mean (SD, min–max) accuracy for congruent trials was 97.3% (3.2, 82–100) and 78.5% (12.6, 35–95) for incongruent trials, a significant difference ($t = 14.9$, $P < 0.0001$). RT was significantly slower ($t = 53$, $P < 0.0001$) in the incongruent [483 ms (41.2, 403–608)] compared with the congruent (386.9 ms (39.4, 281–499) correct trials. Mean median RT for erroneous congruent (61 cases, very few responses) was 386 ms (134.3, 123–743) and 337 ms (34.2, 266–470) for incongruent errors (difference not tested due to few errors in the congruent condition). Stronger ERN amplitude correlated with increased behavioral accuracy in both the congruent ($r = –0.41$, $P < 0.0002$) and the incongruent condition ($r = –0.32$, $P < 0.004$), also when including the effects of age and sex (congruent: $r = –0.41$, $P < 0.0002$, incongruent: $r = –0.36$, $P < 0.002$).

Figure 1B shows the grand averages for correct and erroneous incongruent trials for the 81 participants, demonstrating an ERN in the erroneous trials, while Figure 1C displays the corresponding topographic distribution of the electrophysiological potential; both practically identical to our previous report (Westlye et al. 2009).

Figure 2 depicts the average and the SD of T_1w/T_2w intensity, as well as the per-vertex covariates thickness, and mean curvature for each vertex on the left medial surface. As previously shown (Glasser and Van Essen 2011; Grydeland et al. 2013), areas with high content of myelin such as primary sensory areas show higher T_1w/T_2w ratio. Of note is the variation in both T_1w/T_2w and mean curvature (Fig. 2, lower panel), which might, at least in part, have influenced the intersubject alignment used to identify corresponding surface vertices (see Discussion).

Figure 3A shows the effect of ERN amplitude on T_1w/T_2w intensity across the left cingulate cortex. One left hemisphere cluster showed a significant negative correlation between ERN and T_1w/T_2w, reflecting more negative amplitude with higher T_1w/T_2w intensity [number of vertices = 394, clusterwise *P*-value (CWP) = 0.0002, Talairach X/Y/Z coordinates of maximal *P*-value (Tal X/Y/Z) = –6/–30/34]. The inclusion of FIQ did not affect the relationship (number of vertices = 388, CWP = 0.0002, Tal X/Y/Z = –6/–30/34), neither did the addition of mean curvature as a per-vertex regressor (number of vertices = 403, CWP = 0.0002, Tal X/Y/Z –5/–30/35). Figure 3B shows the ERN amplitude plotted against T_1w/T_2w residuals from the 388 vertices cluster, after controlling for age, sex, FIQ, and cortical thickness ($r = –0.36$).

The assessment of the influence of WM on the intracortical effects showed that the relationship was maintained but reduced when adding WM T_1w/T_2w as a per-vertex regressor (number of vertices = 170, CWP = 0.0292, Tal X/Y/Z = –5/–30/33). The corresponding correlation was $r = –0.33$. In the stepwise regression including WM FA values from the PCC cluster in Westlye et al. and thickness-corrected GM T_1w/T_2w values from the current PCC cluster, the final regression model included both predictors: FA ($\beta = –0.262$, $P = 0.0170$) and T_1w/T_2w ($\beta = –0.249$, $P = 0.0228$). Adjusted R^2 for the final model was 0.16 ($F_{2,78} = 7.67$, $P = 0.00091$), compared with an R^2 of 0.10 for FA only. The Pearson's correlation coefficient between the predictors was 0.2, marginally not significant ($P = 0.074$).

There was no significant correlation between mean T_1w/T_2w in the effect site and correct congruent ($r = –0.13$, $P = 0.265$) or incongruent ($r = –0.03$, $P = 0.770$) RT, nor for RT of incongruent errors ($r = –0.09$, $P = 0.410$), or number of correct congruent ($r = 0.14$, $P = 0.215$) or incongruent ($r = 0.09$, $P = 0.412$) responses. No significant clusters were found in right hemisphere (the lowest CWP was 0.16, in the posterior cingulate cortex). The median correlation between T_1w/T_2w and ERN amplitude across all vertices in the left cingulate were not found to be larger compared with the right ($P = 0.610$).

An exploratory GLM across the entire cortical mantle did not yield any significant clusters after corrections for multiple comparisons; Figure 3C shows the uncorrected *P*-value surface maps. In the left hemisphere, the largest cluster was found in the same posterior cingulate cortex. In the right hemisphere, the largest cluster

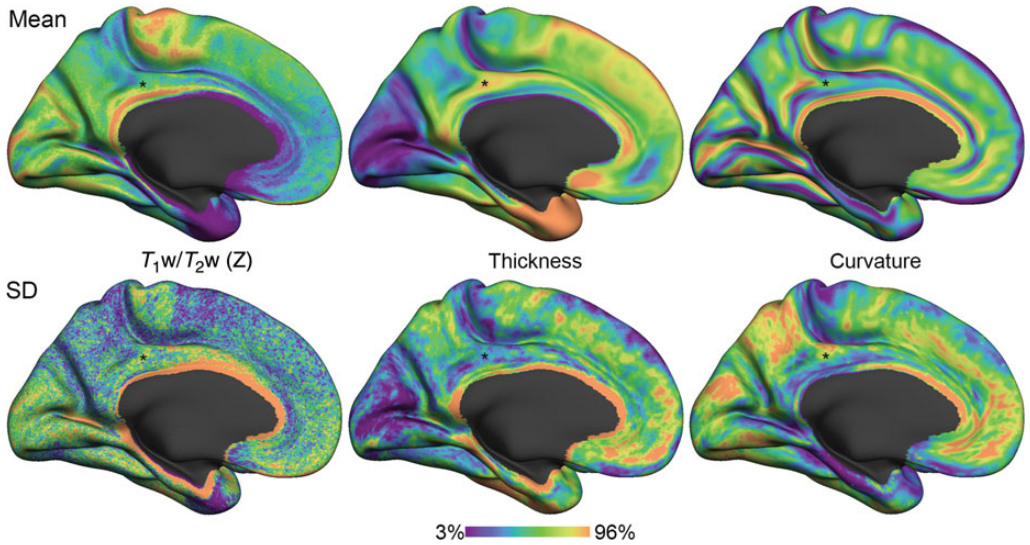

Figure 2. Average and SD of T_1w/T_2w ratio, cortical thickness, and mean curvature across participants. Values are thresholded at 3 and 96 percentile (i.e., values below and above, respectively, were set to color saturation) and were not smoothed before calculation. The units are arbitrary for T_1w/T_2w, mm for thickness, and 1/mm for curvature. The asterisk marks the maximum *P*-value vertex of the T_1w/T_2w-ERN cluster in Figure 3. Colormaps were generated using the *pmkmp* function (Niccoli 2010).

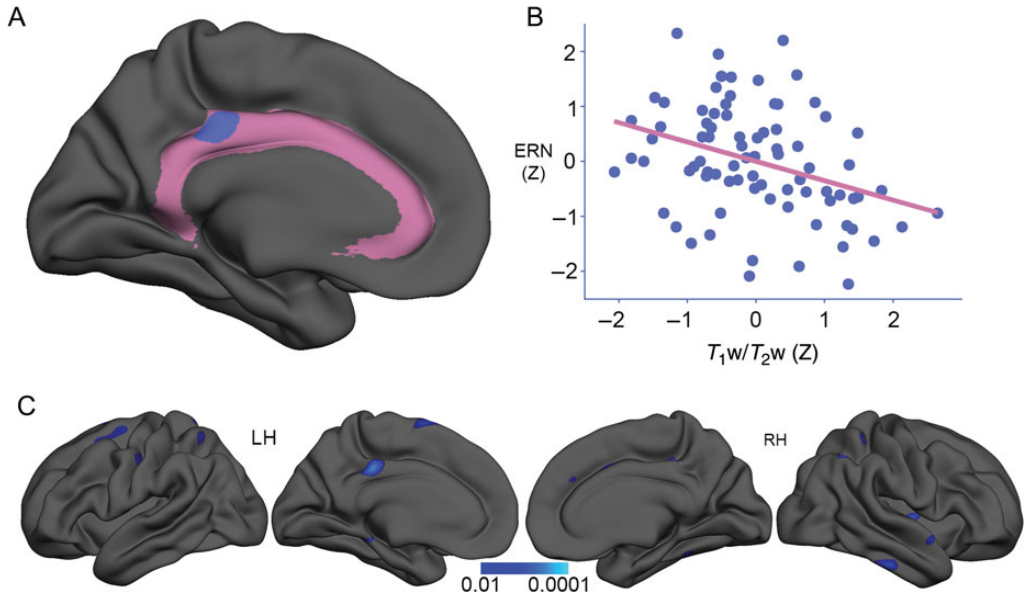

Figure 3. (*A*) Semi-inflated left hemisphere surface rendering showing the T_1w/T_2w-ERN effect site (blue) overlaid the cingulate cortex mask (purple). (*B*) Individual Z scores of ERN amplitude and T_1w/T_2w residuals, after regressing out age, sex, FIQ, and cortical thickness, in the effect site. (*C*) Semi-inflated left (LH) and right hemisphere (RH) surfaces (lateral and medial view) showing *P*-values of tests across the cortical mantle uncorrected for multiple comparisons.

was found in the inferior parietal cortex, although effects were also seen in both anterior and posterior parts of the cingulate cortex. Of note is also the fact that only negative effects were found across hemispheres while we would have expected a random distribution of positive and negative values given under the null distribution, as noted in Westlye et al. (2009). Still, these uncorrected results should be interpreted with caution.

The results of the average T_1w/T_2w values from the overlapping inner half, middle half, and outer half of the GM can be found in Figure 4, which shows uncorrected *P*-values (all clusters except the one marked by the asterisk survived correction for multiple comparisons). In the left hemisphere, the PCC effect was present both for the inner (number of vertices = 510, CWP = 0.0002, Tal X/Y/Z = −5/−30/36) and middle half (number of vertices = 586, CWP = 0.0002, Tal X/Y/Z = −5/−30/36) of the GM, while no effects were observed in the GLM based on the outmost part of the GM. For the right hemisphere, a smaller but similar cluster formed in PCC at 0–50% but did not survive corrections for multiple comparisons (number of vertices = 113, CWP = 0.075, Tal X/Y/Z = 11/−32/39). However, a caudal anterior cingulate cluster was observed (number of vertices = 139, CWP = 0.034, Tal X Y/Z = 9/9/34).

Discussion

Here we demonstrate a link between intracortical myelin and directly measured electrophysiological neural activity. Increased

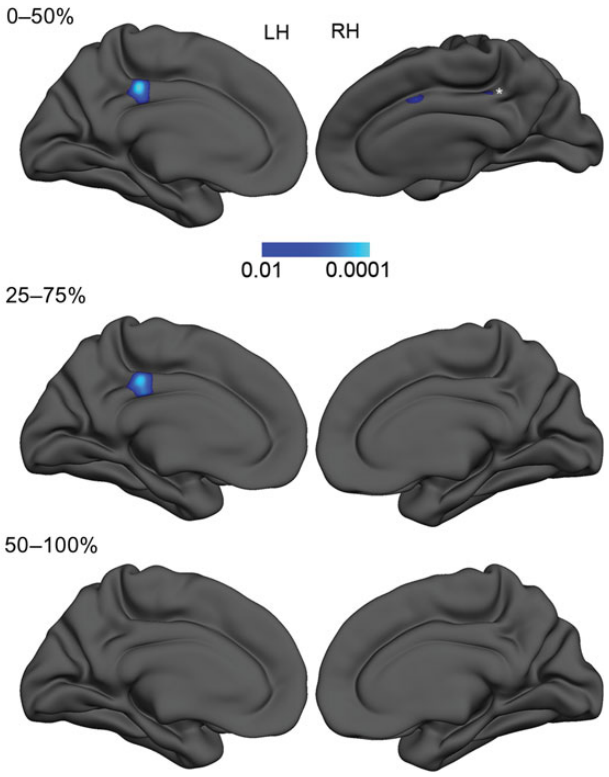

Figure 4. Uncorrected *P*-values of the ERN amplitude effect on average T_1w/T_2w values for the innermost half (from 0% to 50% of the cortical thickness), middle half (from 25% to 50% of the thickness), and outermost half (from 50% to 100% of the thickness) of the cortex. All clusters except for the one indicated by the asterisk survive correction for multiple comparisons at $P = 0.05$. For the right 0–50% results, the hemisphere is tilted for better visualization.

amplitude of the ERP component ERN, a marker of error processing and cognitive control, was related to higher levels of intracortical myelin as measured by T_1w/T_2w signal intensity ratio in the left posterior cingulate cortex. This finding appears in line with the notion that degree of posterior cingulate cortical myelin plays a role in performance monitoring through its relationship with the ERN, potentially by facilitating local neural synchronization. We have previously shown a correlation between posterior cingulate WM microstructure and the amplitude of the ERN (Westlye et al. 2009). However, as the neural generators of electrophysiological markers stem from summated field potentials in the cortex (Luck 2005), the present finding of a relationship with interindividual differences in myelin content within the cortex suggests additional structural effects closer to the generator site.

As hypothesized, the relationship between intracortical T_1w/T_2w intensity and ERN amplitude was located in the cingulate cortex. Specifically, based on Vogt et al. (2006), the observed cluster encompasses the left dorsal posterior cingulate cortex (PCC; anterior parts of Broadman area 23d). PCC connects to a high number of other cortical areas and features prominently in putative core brain networks such as the default mode network (Buckner et al. 2009; van den Heuvel and Sporns 2011). Consequently, PCC has been implicated in a host of processes, preventing simple functional characterizations. Recently, it was proposed that the PCC plays a key role in altering behavior in response to unexpected change (Pearson et al. 2011). This proposal fits recent evidence by Leech et al. (2012), demonstrating that the dorsal PCC relates to distinct distributed networks thought to be closely involved in the control of behavior.

Although agreement exists of cingulate origins of the ERN, the ACC has commonly been attributed as the ERN generator (Dehaene et al. 1994; Debener et al. 2005). Still, source localization of the ERN based on EEG (Mathewson et al. 2005), magnetoencephalography (Keil et al. 2010), simultaneous magneto- and electroencephalography (MEEG) (Miltner et al. 2003), and intracranial recordings (Brazdil et al. 2005; Pourtois et al. 2010), as well as functional MRI studies (Menon et al. 2001; Ullsperger and von Cramon 2001), has shown substantial variation indicating generator and activation sites along large parts of the cingulate cortex in both hemispheres, including the PCC (see for instance Fig. 1 in Agam et al. 2011). Thus, beyond cingulate involvement, consistent findings have been elusive. Of the various source localization methods, MEEG arguably allows for the most accurate localization (Sharon et al. 2007). Our results accord very well with 2 recent source localization studies using MEEG (Agam et al. 2011; Charles et al. 2013); both studies located the source of the ERN to the dorsal PCC bilaterally, peaking in the left hemisphere (Tal *X*/*Y*/*Z* = –6/–19/38, and – 6/–22/33, respectively). Thus, the findings here support the notion that higher levels of intracortical myelin content in the putative generator site dorsal PCC relates to the a neural marker of error processing, which in turn predict response accuracy.

Of note, in Agam et al. (2011), greater functional MRI activation during error trials was observed in the ACC. Additionally, ERN amplitude correlated with fMRI activation in both the PCC and ACC, and the regions showed similar nontask-related fMRI activity, suggesting functional connectivity between the regions, putatively mediated by direct structural connections via the cingulum WM pathway (Vogt et al. 2006). Interestingly, in a second experiment not requiring fast responding, Charles et al. (2013) estimated the ERN source to both the dorsal PCC (Tal *X*/*Y*/*Z* = –9/–23/31) and the dorsal ACC bilaterally (Tal *X*/*Y*/*Z* = 7/2/27). Taken together, these findings suggest that both regions engage in error processing. In accordance with this result, we found a small right ACC cluster in one of the follow-up analysis. A proposed model conjectures that the PCC detects errors, gives rise to the ERN, and then relays error information to the dorsal ACC via the cingulum WM pathway to adapt behavior (Agam et al. 2011). Still, a network of areas probably contributes to error-related processing as for instance ERN amplitude attenuates in patients with lesions not only to the cingulate (Swick and Turken 2002), but also to lateral prefrontal cortex, and basal ganglia nuclei (Ullsperger and von Cramon 2006).

The current effort adds a dimension to our previous WM DTI and ERN investigation using FA as measure of WM cingulum integrity in an overlapping sample (Westlye et al. 2009). The finding of a cortical T_1w/T_2w relationship in the left PCC in the current study fits well with the effect found in Westlye et al., which was situated slightly more posteriorly, in the posterior most part of dorsal PCC, at the border to ventral PCC. Thus, we observe very similar but not identical results using 2 microstructural measures in WM and GM, respectively. Here, the GM finding was still significant after including FA from the abovementioned WM cingulum cluster in our previous study, and, similarly, the GM T_1w/T_2w-ERN effect remained after correction for subjacent WM T_1w/T_2w, although somewhat attenuated. Thus, though FA probably does not mainly reflect myelin (Beaulieu 2002), the significant GM T_1w/T_2w effects after including WM measures appear to suggest at least partially independent contribution from both cortex and WM. In relation to these findings, our main and follow-up analyses indicate that the effects stem from the half of

cortex closest to WM. Low and mid-cortical areas contain fibers both running radial (perpendicular to the surface) and tangential (parallel to the surface); for instance, the horizontal stripes of Baillarger can be seen in low-to-mid-cortical areas in the medial parietal cingulate regions [see for instance Fig. 27 in Nieuwenhuys (2013)]. However, the current resolution precludes determination of whether the effects observed here relate prevalently to local cortical axons or to axons part of long-range connections via deeper WM. Future studies modeling cortical layers using superior image resolution (Waehnert et al. 2014) might disentangle potential independent effects of different connection types.

We cannot exclude the possibility that individual differences in the size of myeloarchitectonic areas, or in the pattern of cortical folding, in part influenced the intersubject alignment used to identify corresponding surface vertices. As evident from Figure 2, and previously reported (Glasser and Van Essen 2011; Grydeland et al. 2013), the T_1w/T_2w-ERN effect is situated in an area of nonuniform distribution of average T_1w/T_2w values, as well as appreciable variation in both T_1w/T_2w and mean curvature (Fig. 2, lower panel). However, we employed a surface-based registration that respects the topology of the cortex despite large individual differences in the convolution patterns, a significant advantage compared with conventional volume-based registration (Fischl et al. 1999; Fischl et al. 2008; Van Essen and Glasser 2014). Local distortion errors might still occur using this approach, most likely in areas of high individual variation such as the ones mentioned above. Still, both individual variation (Fig. 2) and local registration distortion hotspots [see for instance Fig. 1I in Van Essen et al. (2012)] appear more pronounced in other areas both within and outside the cingulate cortex. In addition, when taking local folding patterns into account in our model, the effect remains unchanged. We therefore find this explanation of our results less likely. The agreements with our previous WM-ERN finding and with recent ERN source localization studies further strengthen our belief in the validity of the findings.

Similar to Westlye et al. (2009), we did not observe correlations between brain measures and accuracy, in line with the suggestion that ERPs may constitute an intermediate level linking brain indices and behavior. Agam et al. (2011) did not report correlations between structural indices and accuracy (only self-correction on error trials, a feature not part of the present paradigm), and future studies should address this issue further.

Although 1) T_1w and T_2w intensity patterns have been shown to mainly reflect myeloarchitecture (Eickhoff et al. 2005), 2) high-resolution T_1w images and myelin-stained sections of the same tissue in marmosets accord closely (Bock et al. 2011), and 3) T_1w/T_2w maps have been shown to correspond well with myelin staining maps (Glasser and Van Essen 2011), the contrast mechanism underlying T_1w/T_2w maps is complex. Thus, the T_1w and T_2w images probably reflect other microstructural factors in addition to myelin. Further, the T_1w/T_2w maps do not reflect a quantitative physical property (Glasser et al. 2014), but still demonstrate similar local myeloarchitecture features as maps obtained using quantitative T_1 imaging (Sereno et al. 2013).

In sum, the present result suggests that synchronous neural activity reflecting error processing as measured by the electrophysiological ERN component relates to interindividual variation in intracortical myelin as measured by T_1w/T_2w signal intensity in the left dorsal posterior cingulate cortex. In addition to the implications for our understanding of the neural foundation for error processing and cognitive control per se, the findings indicate that T_1w/T_2w mapping is a sensitive and relevant tool that could be used to address a range of questions related to cognitive and neuropsychiatric deficits in various populations.

Funding

This work was supported by The Norwegian Research Council (to K.B.W., L.T.W. (204966/F20), and A.M.F.), the Department of Psychology, University of Oslo (to H. G., K.B.W. and A.M.F.), and the European Research Council Starting Grant Scheme (to K.B.W. and A.M.F.).

Notes

The current affiliation of L.T.W. is NORMENT K.G. Jebsen Centre for Psychosis Research, Division of Mental Health and Addiction, Oslo University Hospital, Oslo, Norway, and Department of Psychology, University of Oslo. *Conflict of Interest:* None declared.

References

Agam Y, Hamalainen MS, Lee AK, Dyckman KA, Friedman JS, Isom M, Makris N, Manoach DS. 2011. Multimodal neuroimaging dissociates hemodynamic and electrophysiological correlates of error processing. Proc Natl Acad Sci USA. 108:17556–17561.

Beaulieu C. 2002. The basis of anisotropic water diffusion in the nervous system - a technical review. NMR Biomed. 15:435–455.

Beck AT, Steer R. 1987. Beck Depression Inventory scoring manual. New York (NY): The Psychological Corporation.

Bock NA, Hashim E, Kocharyan A, Silva AC. 2011. Visualizing myeloarchitecture with magnetic resonance imaging in primates. Ann NY Acad Sci. 1225(Suppl. 1):E171–E181.

Brazdil M, Roman R, Daniel P, Rektor I. 2005. Intracerebral error-related negativity in a simple Go/NoGo task. J Psychophysiol. 19:244–255.

Brydges CR, Anderson M, Reid CL, Fox AM. 2013. Maturation of cognitive control: delineating response inhibition and interference suppression. PloS ONE. 8:e69826.

Buckner RL, Sepulcre J, Talukdar T, Krienen FM, Liu H, Hedden T, Andrews-Hanna JR, Sperling RA, Johnson KA. 2009. Cortical hubs revealed by intrinsic functional connectivity: mapping, assessment of stability, and relation to Alzheimer's disease. J Neurosci. 29:1860–1873.

Charles L, Van Opstal F, Marti S, Dehaene S. 2013. Distinct brain mechanisms for conscious versus subliminal error detection. Neuroimage. 73:80–94.

Dale AM, Fischl B, Sereno MI. 1999. Cortical surface-based analysis. I. Segmentation and surface reconstruction. Neuroimage. 9:179–194.

Debener S, Ullsperger M, Siegel M, Fiehler K, von Cramon DY, Engel AK. 2005. Trial-by-trial coupling of concurrent electroencephalogram and functional magnetic resonance imaging identifies the dynamics of performance monitoring. J Neurosci. 25:11730–11737.

Dehaene S, Posner MI, Tucker DM. 1994. Localization of a neural system for error detection and compesation. Technical commentary. Psychol Sci. 5:303–305.

Desikan RS, Segonne F, Fischl B, Quinn BT, Dickerson BC, Blacker D, Buckner RL, Dale AM, Maguire RP, Hyman BT, et al. 2006. An automated labeling system for subdividing the human cerebral cortex on MRI scans into gyral based regions of interest. Neuroimage. 31:968–980.

Eickhoff S, Walters NB, Schleicher A, Kril J, Egan GF, Zilles K, Watson JD, Amunts K. 2005. High-resolution MRI reflects myeloarchitecture and cytoarchitecture of human cerebral cortex. Hum Brain Mapp. 24:206–215.

Elvsashagen T, Moberget T, Boen E, Hol PK, Malt UF, Andersson S, Westlye LT. 2014. The surface area of early visual cortex predicts the amplitude of the visual evoked potential. Brain Struct Funct. 220:1229–1236.

Falkenstein M, Hohnsbein J, Hoormann J, Blanke L. 1991. Effects of crossmodal divided attention on late ERP components. II. Error processing in choice reaction tasks. Electroencephalogr Clin Neurophysiol. 78:447–455.

Fischl B, Dale AM. 2000. Measuring the thickness of the human cerebral cortex from magnetic resonance images. Proc Natl Acad Sci USA. 97:11050–11055.

Fischl B, Rajendran N, Busa E, Augustinack J, Hinds O, Yeo BT, Mohlberg H, Amunts K, Zilles K. 2008. Cortical folding patterns and predicting cytoarchitecture. Cereb Cortex. 18:1973–1980.

Fischl B, Sereno MI, Tootell RB, Dale AM. 1999. High-resolution intersubject averaging and a coordinate system for the cortical surface. Hum Brain Mapp. 8:272–284.

Folstein MF, Folstein SE, McHugh PR. 1975. "Mini-mental state". A practical method for grading the cognitive state of patients for the clinician. J Psychiatr Res. 12:189–198.

Gehring WJ, Goss B, Coles MGH, Meyer DE, Donchin E. 1993. A neural system for error detection and compensation. Psychol Sci. 4:385–390.

Girard P, Hupe JM, Bullier J. 2001. Feedforward and feedback connections between areas V1 and V2 of the monkey have similar rapid conduction velocities. J Neurophysiol. 85: 1328–1331.

Glasser MF, Goyal MS, Preuss TM, Raichle ME, Van Essen DC. 2014. Trends and properties of human cerebral cortex: correlations with cortical myelin content. Neuroimage. 93(Pt 2):165–175.

Glasser MF, Van Essen DC. 2011. Mapping human cortical areas in vivo based on myelin content as revealed by T1- and T2-weighted MRI. J Neurosci. 31:11597–11616.

Greve DN, Fischl B. 2009. Accurate and robust brain image alignment using boundary-based registration. Neuroimage. 48:63–72.

Grydeland H, Walhovd KB, Tamnes CK, Westlye LT, Fjell AM. 2013. Intracortical myelin links with performance variability across the human lifespan: results from T1- and T2-weighted MRI myelin mapping and diffusion tensor imaging. J Neurosci. 33:18618–18630.

Hagler DJ Jr, Saygin AP, Sereno MI. 2006. Smoothing and cluster thresholding for cortical surface-based group analysis of fMRI data. Neuroimage. 33:1093–1103.

Hauser TU, Iannaccone R, Stampfli P, Drechsler R, Brandeis D, Walitza S, Brem S. 2014. The feedback-related negativity (FRN) revisited: new insights into the localization, meaning and network organization. Neuroimage. 84:159–168.

Hildebrand C, Remahl S, Persson H, Bjartmar C. 1993. Myelinated nerve fibres in the CNS. Progr Neurobiol. 40:319–384.

Keil J, Weisz N, Paul-Jordanov I, Wienbruch C. 2010. Localization of the magnetic equivalent of the ERN and induced oscillatory brain activity. Neuroimage. 51:404–411.

Leech R, Braga R, Sharp DJ. 2012. Echoes of the brain within the posterior cingulate cortex. J Neurosci. 32:215–222.

Luck SJ. 2005. An introduction to the event-related potential technique. Cambridge (MA): The MIT Press.

Mathewson KJ, Dywan J, Segalowitz SJ. 2005. Brain bases of error-related ERPs as influenced by age and task. Biol Psychol. 70:88–104.

Menon V, Adleman NE, White CD, Glover GH, Reiss AL. 2001. Error-related brain activation during a Go/NoGo response inhibition task. Hum Brain Mapp. 12:131–143.

Miltner WH, Lemke U, Weiss T, Holroyd C, Scheffers MK, Coles MG. 2003. Implementation of error-processing in the human anterior cingulate cortex: a source analysis of the magnetic equivalent of the error-related negativity. Biol Psychol. 64:157–166.

Nave KA. 2010. Myelination and support of axonal integrity by glia. Nature. 468:244–252.

Niccoli M. 2010. Perceptually improved colormaps. In: MATLAB Central File Exchange. http://www.mathworks.com/matlabcentral/fileexchange/28982, Retrieved September 17, 2014.

Nieuwenhuys R. 2013. The myeloarchitectonic studies on the human cerebral cortex of the Vogt-Vogt school, and their significance for the interpretation of functional neuroimaging data. Brain Struct Funct. 218:303–352.

Palm G, Knoblauch A, Hauser F, Schuz A. 2014. Cell assemblies in the cerebral cortex. Biol Cybern. 108:559–572.

Pearson JM, Heilbronner SR, Barack DL, Hayden BY, Platt ML. 2011. Posterior cingulate cortex: adapting behavior to a changing world. Trend Cogn Sci. 15:143–151.

Poulsen C, Picton TW, Paus T. 2007. Age-related changes in transient and oscillatory brain responses to auditory stimulation in healthy adults 19–45 years old. Cereb Cortex. 17:1454–1467.

Pourtois G, Vocat R, N'Diaye K, Spinelli L, Seeck M, Vuilleumier P. 2010. Errors recruit both cognitive and emotional monitoring systems: simultaneous intracranial recordings in the dorsal anterior cingulate gyrus and amygdala combined with fMRI. Neuropsychologia. 48:1144–1159.

Semlitsch HV, Anderer P, Schuster P, Presslich O. 1986. A solution for reliable and valid reduction of ocular artifacts, applied to the P300 ERP. Psychophysiology. 23:695–703.

Sereno MI, Lutti A, Weiskopf N, Dick F. 2013. Mapping the human cortical surface by combining quantitative T(1) with retinotopy. Cereb Cortex. 23:2261–2268.

Sharon D, Hamalainen MS, Tootell RB, Halgren E, Belliveau JW. 2007. The advantage of combining MEG and EEG: comparison to fMRI in focally stimulated visual cortex. Neuroimage. 36:1225–1235.

Swick D, Turken AU. 2002. Dissociation between conflict detection and error monitoring in the human anterior cingulate cortex. Proc Natl Acad Sci USA. 99:16354–16359.

Taylor SF, Stern ER, Gehring WJ. 2007. Neural systems for error monitoring: recent findings and theoretical perspectives. Neuroscientist. 13:160–172.

Thatcher RW, Biver C, McAlaster R, Camacho M, Salazar A. 1998. Biophysical linkage between MRI and EEG amplitude in closed head injury. Neuroimage. 7:352–367.

Thomson AM, Bannister AP. 2003. Interlaminar connections in the neocortex. Cereb Cortex. 13:5–14.

Tomassy GS, Berger DR, Chen HH, Kasthuri N, Hayworth KJ, Vercelli A, Seung HS, Lichtman JW, Arlotta P. 2014. Distinct profiles of myelin distribution along single axons of pyramidal neurons in the neocortex. Science. 344:319–324.

Ullsperger M, von Cramon DY. 2006. The role of intact frontostriatal circuits in error processing. J Cogn Neurosci. 18:651–664.

Ullsperger M, von Cramon DY. 2001. Subprocesses of performance monitoring: a dissociation of error processing and response competition revealed by event-related fMRI and ERPs. Neuroimage. 14:1387–1401.

van den Heuvel MP, Sporns O. 2011. Rich-club organization of the human connectome. J Neurosci. 31:15775–15786.

Van Essen DC, Glasser MF. 2014. In vivo architectonics: a cortico-centric perspective. Neuroimage. 93(Pt 2):157–164.
Van Essen DC, Glasser MF, Dierker DL, Harwell J, Coalson T. 2012. Parcellations and hemispheric asymmetries of human cerebral cortex analyzed on surface-based atlases. Cereb Cortex. 22:2241–2262.
Varela F, Lachaux JP, Rodriguez E, Martinerie J. 2001. The brainweb: phase synchronization and large-scale integration. Nat Rev Neurosci. 2:229–239.
Voges N, Schuz A, Aertsen A, Rotter S. 2010. A modeler's view on the spatial structure of intrinsic horizontal connectivity in the neocortex. Progr Neurobiol. 92:277–292.
Vogt BA, Vogt L, Laureys S. 2006. Cytology and functionally correlated circuits of human posterior cingulate areas. Neuroimage. 29:452–466.
Waehnert MD, Dinse J, Weiss M, Streicher MN, Waehnert P, Geyer S, Turner R, Bazin PL. 2014. Anatomically motivated modeling of cortical laminae. Neuroimage. 93(Pt 2): 210–220.
Wechsler D. 1999. Wechsler Abbreviated Scale of Intelligence. San Antonio (TX): The Psychological Corporation.
Westlye LT, Walhovd KB, Bjornerud A, Due-Tonnessen P, Fjell AM. 2009. Error-related negativity is mediated by fractional anisotropy in the posterior cingulate gyrus–a study combining diffusion tensor imaging and electrophysiology in healthy adults. Cereb Cortex. 19:293–304.
Westlye LT, Walhovd KB, Dale AM, Bjornerud A, Due-Tonnessen P, Engvig A, Grydeland H, Tamnes CK, Ostby Y, Fjell AM. 2010. Differentiating maturational and aging-related changes of the cerebral cortex by use of thickness and signal intensity. Neuroimage. 52:172–185.
Yeung N, Cohen JD, Botvinick MM. 2004. The neural basis of error detection: conflict monitoring and the error-related negativity. Psychol Rev. 111:931–959.